

Order of Accuracy Analysis

Sourabh P. Bhat

<https://spbhat.in>

December 10, 2019

The truncation error of a numerical method is dependent on the grid spacing. That is, every time we reduce the grid spacing (cell size), the truncation error is expected to reduce. This can be observed theoretically by carrying out a Taylor's series expansion of the numerical scheme and subtracting the result from the exact partial differential equation. The residue left out is the truncation error, which can be written as,

$$\epsilon = c_0 (\Delta x)^{\mathcal{O}} + c_1 (\Delta x)^{\mathcal{O}+1} + c_2 (\Delta x)^{\mathcal{O}+2} \dots \quad (1)$$

where, c_i ; $i = 0, 1, 2 \dots$ are coefficients which are independent of cell size. Neglecting the higher order terms (since Δx is small), we get,

$$\epsilon \approx c_0 (\Delta x)^{\mathcal{O}} \implies \epsilon \propto (\Delta x)^{\mathcal{O}} \quad (2)$$

The order of such a scheme is said to be \mathcal{O} . It may not be always possible to carry out a theoretical analysis of a non-linear method, such as in the case of SDWLS, WENO or limiter based methods. In such schemes the formulation is dependent on the solution and thus, a priori Taylor's series expansion is not possible. This calls for a numerical approach for obtaining the order of accuracy of the scheme. To carry out the numerical analysis, of order of accuracy, we can write equation (2) for two cell sizes, say Δx_1 and Δx_2 and the corresponding errors as ϵ_1 and ϵ_2 . This results in the following two equations,

$$\epsilon_1 \propto (\Delta x_1)^{\mathcal{O}} \quad (3)$$

$$\epsilon_2 \propto (\Delta x_2)^{\mathcal{O}} \quad (4)$$

Now, dividing equation (4) by equation (3) results in the following equation,

$$\frac{\epsilon_2}{\epsilon_1} = \left(\frac{\Delta x_2}{\Delta x_1} \right)^{\mathcal{O}} \implies \log(\epsilon_2) - \log(\epsilon_1) = \mathcal{O} \cdot (\log(\Delta x_2) - \log(\Delta x_1)) \quad (5)$$

Rearranging this equation, we get an expression for the order of accuracy as,

$$\mathcal{O} = \frac{\log(\epsilon_2) - \log(\epsilon_1)}{\log(\Delta x_2) - \log(\Delta x_1)} \quad (6)$$

This can be observed as the slope of a curve on a log-log plot of error versus cell size. It may be noted that the Δx is a measure of the cell size, and for a two-dimensional Cartesian mesh it is appropriately defined as,

$$h = \sqrt{\Delta x \Delta y} \quad (7)$$

In case of unstructured mesh, the measure of cell size is defined by the average of all the cells in the domain, which can be defined as,

$$h = \sqrt{\frac{\text{area of domain}}{\text{total number of cells}}} \quad (8)$$

and therefore, the order of accuracy of the method for a two-dimensional problem gets redefined as,

$$\mathcal{O} = \frac{\log(\epsilon_2) - \log(\epsilon_1)}{\log(h_2) - \log(h_1)} \quad (9)$$

An order of accuracy analysis is a systematic process in which the error is obtained for various cell sizes. The error versus cell size is then plotted on a log-log plot. The actual order is obtained by calculating the slope of the curve on this plot. It has been pointed out by Toro [1], that the order of accuracy may not be apparent in case of non-linear schemes. It is therefore essential to carry out the order of accuracy analysis of new schemes before using them. In my work, I have computed numerically the order of accuracy of the following solution reconstruction methods: first order, Beam-Warming scheme using van Albada limiter, linear and quadratic SDWLS, third order and fifth order WENO method. The analysis has been conducted for various problems in one-dimension and two-dimensions on a structured and unstructured mesh.

1 Review of Literature

The Godunov theorem [2] states that it is not possible for a linear higher order scheme, (of order two or higher), to ensure a non-oscillatory solution. It is however observed that, if there are no discontinuities in the solution then, the numerical solution obtained by a linear high order scheme is much superior compared to the first order upwind scheme. It has been a quest of many researches to circumvent the limitation imposed by the Godunov theorem to achieve an order of accuracy as high as possible. This effort has led to two classes of methods of adding non-linearity to the scheme. The two classes of methods are: the artificial viscosity methods and the total variation diminishing methods. In case of artificial viscosity methods [3] additional non-physical, viscous like terms, are added to the scheme such that the oscillations are damped out. The currently available methods in this class, have to define a coefficient which has to be tuned according to the problem. Therefore, these methods are not easily extensible to general problems. The total variation diminishing (TVD) methods include slope-limiters and flux-limiters to locally switch to a lower order, based on the local gradients. This class of methods are more general to extend to any type of problems and therefore are more widely used. Many major contributions have been made to this class of methods over the years [?, 4–10]. Various limiters have been defined which perform identically far away from the discontinuity but change their behavior close to the region of high gradients. The limiter versus the gradient-ratio plot commonly known as Sweby plot [9] is used in these methods to define a limiter function. Some of the widely used limiter functions are SUPERBEE [11], VANLEER [4], VANALBADA [12], MINMOD [13].

A hybrid class of schemes closely related to TVD methods are solution dependent methods. In these methods a MUSCL-type [14] solution strategy is used, with a linear combination of all possible solution reconstructions. MUSCL stands for Monotone Upstream-centered Scheme

for Conservation Laws. These type of methods include a family of more recent methods like SDWLS [15, 16] and WENO [17] methods. The combination of weights is so chosen, such that it reduces the oscillations. These methods do not enforce the TVD condition explicitly, and therefore may encounter oscillations within acceptable limits. In the SDWLS method, each of the neighboring cells are expressed as a function of the cell value and derivatives, using Taylor's series expansion, about the cell's centroid. This results in a system of equations with the derivatives as unknowns. Now, this system of equations are solved for the derivatives in a least-square sense, after application of weights. The weights are inversely proportional to the variation from the central cell, thus reducing the oscillations. The WENO method uses an approach where, all the candidate stencils are reconstructed. Appropriate weights are then applied to each of the stencil solutions based on the smoothness in the stencil.

The current trends in high order methods and their need are very well reviewed by Wang and group in their article [18]. The order of accuracy analysis of WENO methods for structured grids is performed by Balsara [19]. The analysis on unstructured grid for WENO methods is carried out by Hu [20] and Liu [21]. Using the ADER approach (Arbitrary high-order DERivative Riemann problem) and discontinuous Galerkin finite element method, the analysis has been performed by Dumbser et al. [22, 23].

2 Need of High Order Methods

The goal being that we need to achieve some level of accuracy, say 10^{-3} of absolute error, we may ask ourselves the following question. Are high order methods really required? or is it more efficient to solve the problem on a very fine mesh using a first order method? It is well known that a first order method will run much faster than a second order method on a given mesh. But if we keep refining the mesh until the first order method achieves similar solution as second order method, will the first order method still take lesser time? The following simple demonstration tries to answer this question by actually solving a problem on various uniformly refined grids and comparing the computational time and memory requirement. The problem being solved here is a simple advection equation (10), initialized with a smooth sine function (11) having a wave number of unity (see Figure 1). The boundary conditions are periodic and thus the final exact solution after 1 complete cycle is same as the initial distribution. The domain length chosen is 2 ranging from -1 to $+1$.

$$u_t + u_x = 0 \quad (10)$$

$$u_0 = u(x, t = 0) = \sin(2\pi x) \quad (11)$$

Using a trial and error method, the number of grid cells required by the second order method is estimated. To achieve an L_2 -error of approximately 10^{-3} , the second order method requires 320 cells as seen in Table 1. Whereas, the first order method takes a phenomenal amount of cells, about 128 times more, as seen in Table 2, and therefore a proportionally large amount of memory. An even more appealing advantage of high-order methods can be observed by comparing the time taken. To achieve a similar L_2 -error, approximately 10^{-3} , the first order method takes more than 20,000 times more computational time!. This overwhelming difference is observed due to two reasons. The first reason is obviously due to the higher number of mesh cells required by the first order method. The second reason is most probably the limited cache on the machine which caused repeated cache flushing. This efficiency gap between an

Grid Size	L_2 Error (Absolute)	Compute Time ($\times 10^{-3}$ seconds)
80	1.8518×10^{-2}	~ 20
160	4.5853×10^{-3}	~ 30
320	1.1431×10^{-3}	~ 80
640	2.8555×10^{-4}	~ 200
1280	7.1374×10^{-5}	~ 700
2560	1.7842×10^{-5}	~ 1800
5120	4.4606×10^{-6}	~ 7000
10240	1.1152×10^{-6}	~ 35000

Table 1: Error and computational time for Fromm (second order) method

Grid Size	L_2 Error (Absolute)	Compute Time ($\times 10^{-3}$ seconds)
10240	5.4313×10^{-3}	~ 20000
20480	2.7209×10^{-3}	~ 300000
40960	1.3617×10^{-3}	~ 1735000

Table 2: Error and computational time for first order upwind method

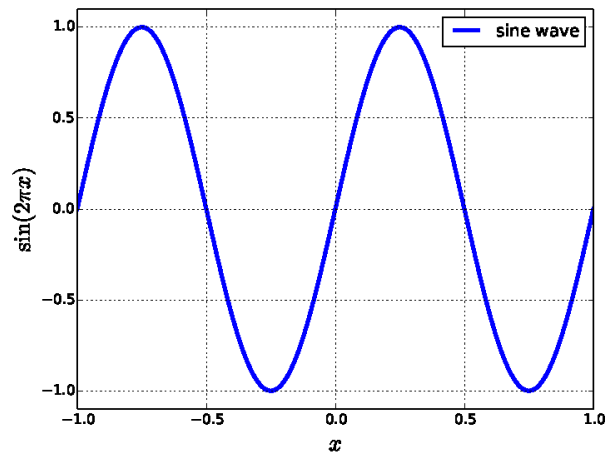


Figure 1: Sine distribution with wave number = 1

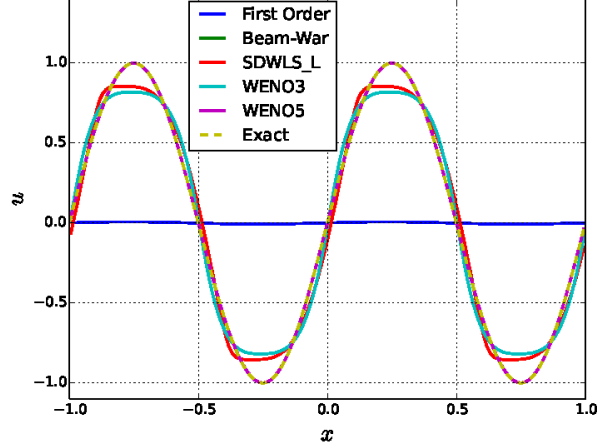


Figure 2: Solution of advection equation for sine function (160 cells)

high order method and a lower order method grows as we demand for more and more accurate results. Thus, this small experiment makes it obvious that, we must try to use higher order methods whenever possible. There are however, two major difficulties associated with high-order methods. The first difficulty is due to the oscillations which appear in the solutions. The second difficulty is associated with the stability of the methods. The TVD, SDWLS and WENO methods try to overcome these difficulties by using a non-linear solution dependent approach.

3 Results and Discussion

Few standard problems are considered here for ascertaining the order of accuracy. The methods for which the order is computed and compared include: first order, second order Beam-Warming using van Albada limiter, SDWLS-L (linear SDWLS), SDWLS-Q (quadratic SDWLS), WENO3 (third order WENO) and WENO5 (fifth order WENO).

3.1 One-Dimensional Problems

3.1.1 Smooth sinusoidal distribution

The initial condition considered here is a sine distribution as shown in [Figure 1](#). The number of grid cells is increased gradually from 20 up to 320. The final solution after 10 cycles (with $CFL = 0.6$) is shown in [Figure 2](#) for all tested reconstruction methods and a grid size of 160 cells. The order of accuracy, as given by equation (6), is calculated after 1 cycle (with $CFL = 0.1$) and is tabulated in [Table 3](#) through [Table 7](#).

3.1.2 Smooth Gaussian distribution

In this problem the initial condition considered is a smooth Gaussian distribution (12) as shown in [Figure 3](#). The number of grid cells is increased gradually from 20 up to 320. The final solution after 10 cycles (with $CFL = 0.6$) is shown in [Figure 4](#) for all tested reconstruction methods and a grid size of 160 cells. The order of accuracy, as given by equation (6), is calculated after 1 cycle

Grid Size	L_1 Error	L_1 Order	L_2 Error	L_2 Order	L_∞ Error	L_∞ Order
20	6.3783×10^{-1}	–	6.9694×10^{-1}	–	9.8550×10^{-1}	–
40	5.5120×10^{-1}	0.211	6.1006×10^{-1}	0.192	8.5619×10^{-1}	0.203
80	3.9969×10^{-1}	0.464	4.4370×10^{-1}	0.459	6.2677×10^{-1}	0.450
160	2.4798×10^{-1}	0.689	2.7543×10^{-1}	0.688	3.8944×10^{-1}	0.687
320	1.3920×10^{-1}	0.833	1.5461×10^{-1}	0.833	2.1865×10^{-1}	0.833

Table 3: Accuracy analysis (sine wave) for First Order Scheme

Grid Size	L_1 Error	L_1 Order	L_2 Error	L_2 Order	L_∞ Error	L_∞ Order
20	4.3153×10^{-1}	–	4.7967×10^{-1}	–	7.0460×10^{-1}	–
40	1.2665×10^{-1}	1.769	1.5824×10^{-1}	1.600	2.7562×10^{-1}	1.354
80	5.3284×10^{-2}	1.249	6.0653×10^{-2}	1.383	1.0793×10^{-1}	1.353
160	1.4431×10^{-2}	1.885	1.8485×10^{-2}	1.714	4.1907×10^{-2}	1.365
320	3.6118×10^{-3}	1.998	5.4723×10^{-3}	1.756	1.5835×10^{-2}	1.404

Table 4: Accuracy analysis (sine wave) for Beam-Warming Scheme

Grid Size	L_1 Error	L_1 Order	L_2 Error	L_2 Order	L_∞ Error	L_∞ Order
20	4.3705×10^{-1}	–	4.8630×10^{-1}	–	7.1521×10^{-1}	–
40	1.2749×10^{-1}	1.777	1.5975×10^{-1}	1.606	2.7804×10^{-1}	1.363
80	5.3672×10^{-2}	1.248	6.1084×10^{-2}	1.387	1.0862×10^{-1}	1.356
160	1.4500×10^{-2}	1.888	1.8587×10^{-2}	1.717	4.2099×10^{-2}	1.367
320	3.6250×10^{-3}	2.000	5.4955×10^{-3}	1.758	1.5876×10^{-2}	1.407

Table 5: Accuracy analysis (sine wave) for SDWLS-Linear Scheme

Grid Size	L_1 Error	L_1 Order	L_2 Error	L_2 Order	L_∞ Error	L_∞ Order
20	4.7010×10^{-1}	–	5.2244×10^{-1}	–	7.6135×10^{-1}	–
40	1.5456×10^{-1}	1.605	1.9506×10^{-1}	1.421	3.2949×10^{-1}	1.208
80	6.6494×10^{-2}	1.217	7.5612×10^{-2}	1.367	1.3149×10^{-1}	1.325
160	1.6817×10^{-2}	1.983	2.3098×10^{-2}	1.711	5.1299×10^{-2}	1.358
320	3.3952×10^{-3}	2.308	5.7918×10^{-3}	1.996	1.6663×10^{-2}	1.622

Table 6: Accuracy analysis (sine wave) for third order WENO Scheme

Grid Size	L_1 Error	L_1 Order	L_2 Error	L_2 Order	L_∞ Error	L_∞ Order
20	5.4333×10^{-2}	–	6.0128×10^{-2}	–	8.6949×10^{-2}	–
40	2.8407×10^{-3}	4.257	3.1719×10^{-3}	4.245	4.5297×10^{-3}	4.263
80	9.0664×10^{-5}	4.970	1.0420×10^{-4}	4.928	1.6812×10^{-4}	4.752
160	2.9530×10^{-6}	4.940	3.3420×10^{-6}	4.962	5.6386×10^{-6}	4.898
320	1.0732×10^{-7}	4.782	1.2000×10^{-7}	4.800	1.9843×10^{-7}	4.829

Table 7: Accuracy analysis (sine wave) for fifth order WENO Scheme

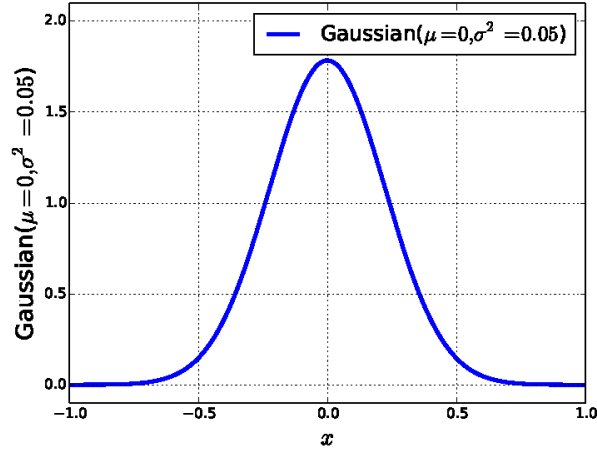


Figure 3: Gaussian distribution with $\mu = 0, \sigma^2 = 0.05$

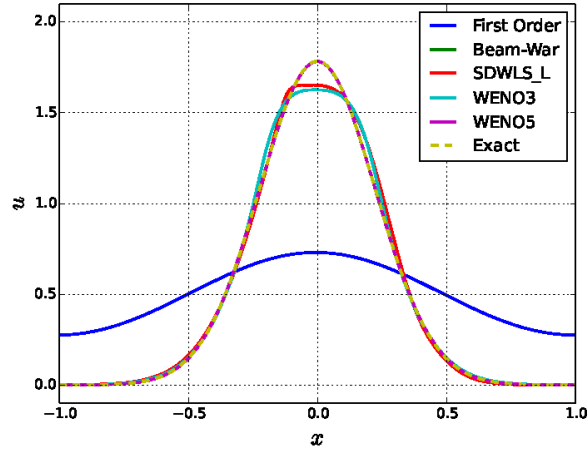


Figure 4: Solution of advection equation for a Gaussian function (160 cells)

(with $CFL = 0.1$) and is tabulated in [Table 8](#) through [Table 12](#).

$$G(\mu, \sigma) = f(x) = a e^{-\frac{(x-\mu)^2}{2\sigma^2}}; a = \frac{1}{\sigma\sqrt{2\pi}}; \mu = 0; \sigma^2 = 0.05 \quad (12)$$

3.1.3 Distribution with various sub-functions

In this problem the initial condition considered is a complicated function (13) comprising of various sub-functions as shown in [Figure 5](#). The number of grid cells is increased gradually from 20 up to 320. The final solution after 10 cycles (with $CFL = 0.6$) is shown in [Figure 6](#) for all tested reconstruction methods and a grid size of 160 cells. The order of accuracy, as given by equation (6), is calculated after 1 cycle (with $CFL = 0.1$) and is tabulated in [Table 8](#) through

Grid Size	L_1 Error	L_1 Order	L_2 Error	L_2 Order	L_∞ Error	L_∞ Order
20	3.7118×10^{-1}	–	4.4005×10^{-1}	–	9.5286×10^{-1}	–
40	2.5937×10^{-1}	0.517	3.2232×10^{-1}	0.449	7.4809×10^{-1}	0.349
80	1.6605×10^{-1}	0.643	2.1632×10^{-1}	0.575	5.2166×10^{-1}	0.520
160	9.7763×10^{-2}	0.764	1.3205×10^{-1}	0.712	3.2727×10^{-1}	0.673
320	5.3936×10^{-2}	0.858	7.4542×10^{-2}	0.825	1.8834×10^{-1}	0.797

Table 8: Accuracy analysis (Gaussian) for First Order Scheme

Grid Size	L_1 Error	L_1 Order	L_2 Error	L_2 Order	L_∞ Error	L_∞ Order
20	1.3888×10^{-1}	–	1.9387×10^{-1}	–	4.8635×10^{-1}	–
40	4.4164×10^{-2}	1.653	7.6203×10^{-2}	1.347	2.3214×10^{-1}	1.067
80	1.4258×10^{-2}	1.631	2.7112×10^{-2}	1.491	9.7092×10^{-2}	1.258
160	3.9880×10^{-3}	1.838	8.5159×10^{-3}	1.671	3.8131×10^{-2}	1.348
320	1.0168×10^{-3}	1.972	2.5281×10^{-3}	1.752	1.4450×10^{-2}	1.400

Table 9: Accuracy analysis (Gaussian) for Beam-Warming Scheme

Grid Size	L_1 Error	L_1 Order	L_2 Error	L_2 Order	L_∞ Error	L_∞ Order
20	1.4003×10^{-1}	–	1.9542×10^{-1}	–	4.9070×10^{-1}	–
40	4.4487×10^{-2}	1.654	7.6694×10^{-2}	1.349	2.3373×10^{-1}	1.070
80	1.4329×10^{-2}	1.635	2.7262×10^{-2}	1.492	9.7635×10^{-2}	1.259
160	4.0017×10^{-3}	1.840	8.5584×10^{-3}	1.671	3.8297×10^{-2}	1.350
320	1.0195×10^{-3}	1.973	2.5416×10^{-3}	1.752	1.4514×10^{-2}	1.400

Table 10: Accuracy analysis (Gaussian) for SDWLS-Linear Scheme

Grid Size	L_1 Error	L_1 Order	L_2 Error	L_2 Order	L_∞ Error	L_∞ Order
20	1.5893×10^{-1}	–	2.1619×10^{-1}	–	5.3957×10^{-1}	–
40	5.3341×10^{-2}	1.575	8.6013×10^{-2}	1.330	2.6760×10^{-1}	1.012
80	1.6307×10^{-2}	1.710	3.2844×10^{-2}	1.389	1.1658×10^{-1}	1.199
160	4.0067×10^{-3}	2.025	1.0383×10^{-2}	1.661	4.5883×10^{-2}	1.345
320	7.8063×10^{-4}	2.360	2.5753×10^{-3}	2.011	1.4741×10^{-2}	1.638

Table 11: Accuracy analysis (Gaussian) for third order WENO Scheme

Grid Size	L_1 Error	L_1 Order	L_2 Error	L_2 Order	L_∞ Error	L_∞ Order
20	2.0664×10^{-2}	–	3.0251×10^{-2}	–	8.7248×10^{-2}	–
40	1.7346×10^{-3}	3.574	2.5299×10^{-3}	3.580	5.9983×10^{-3}	3.862
80	7.2286×10^{-5}	4.585	1.0558×10^{-4}	4.583	2.8730×10^{-4}	4.384
160	2.6672×10^{-6}	4.760	3.7430×10^{-6}	4.818	1.1333×10^{-5}	4.664
320	1.7407×10^{-7}	3.938	5.3205×10^{-7}	2.815	5.2724×10^{-6}	1.104

Table 12: Accuracy analysis (Gaussian) for fifth order WENO Scheme

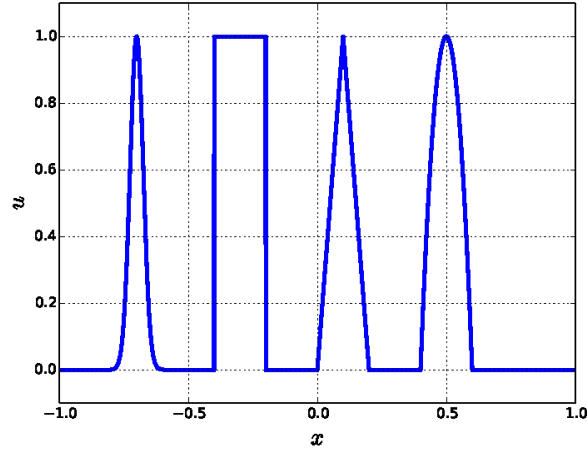


Figure 5: Combination of various functions

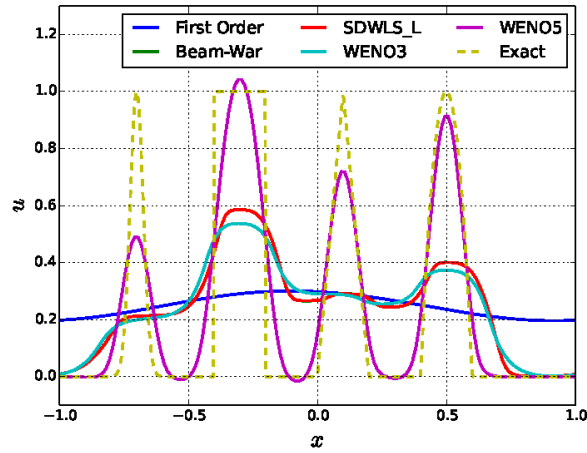


Figure 6: Solution of advection equation for a combination of functions (160 cells)

Table 12.

$$F(x) = \begin{cases} \exp\left(-\frac{10000}{9} \ln(2) (2(x_r - 0.15))^2\right) & 0.1 \leq x_r \leq 0.2 \\ 1 & 0.3 \leq x_r \leq 0.4 \\ 1 - 20|x_r - 0.55| & 0.5 \leq x_r \leq 0.6 \\ 1 - 100(2(x_r - 0.75))^2 & 0.7 \leq x_r \leq 0.8 \\ 0 & \text{otherwise} \end{cases} \quad x_r = \frac{x - x_{min}}{x_{max} - x_{min}} \quad (13)$$

3.2 Two-Dimensional Scalar Problems

A two-dimensional scalar advection equation may be written as,

$$u_t + u_x + u_y = 0 \quad (14)$$

Grid Size	L_1 Error	L_1 Order	L_2 Error	L_2 Order	L_∞ Error	L_∞ Order
20	2.8497×10^{-1}	–	3.3803×10^{-1}	–	7.1802×10^{-1}	–
40	3.0359×10^{-1}	-0.091	3.5332×10^{-1}	-0.064	7.0380×10^{-1}	0.029
80	2.9221×10^{-1}	0.055	3.5076×10^{-1}	0.010	7.1532×10^{-1}	-0.023
160	2.7212×10^{-1}	0.103	3.3114×10^{-1}	0.083	7.8758×10^{-1}	-0.139
320	2.2939×10^{-1}	0.246	2.8575×10^{-1}	0.213	7.6753×10^{-1}	0.037

Table 13: Accuracy analysis (13) for First Order Scheme

Grid Size	L_1 Error	L_1 Order	L_2 Error	L_2 Order	L_∞ Error	L_∞ Order
20	2.5910×10^{-1}	–	3.1750×10^{-1}	–	6.3457×10^{-1}	–
40	2.6976×10^{-1}	-0.058	3.2795×10^{-1}	-0.047	6.0818×10^{-1}	0.061
80	2.0021×10^{-1}	0.430	2.5518×10^{-1}	0.362	6.4868×10^{-1}	-0.093
160	1.0248×10^{-1}	0.966	1.5853×10^{-1}	0.687	5.7906×10^{-1}	0.164
320	4.8108×10^{-2}	1.091	1.0118×10^{-1}	0.648	5.1687×10^{-1}	0.164

Table 14: Accuracy analysis (13) for Beam-Warming Scheme

Grid Size	L_1 Error	L_1 Order	L_2 Error	L_2 Order	L_∞ Error	L_∞ Order
20	2.5931×10^{-1}	–	3.1805×10^{-1}	–	6.3881×10^{-1}	–
40	2.7021×10^{-1}	-0.059	3.2851×10^{-1}	-0.047	6.0848×10^{-1}	0.070
80	2.0076×10^{-1}	0.429	2.5574×10^{-1}	0.361	6.5000×10^{-1}	-0.095
160	1.0265×10^{-1}	0.968	1.5873×10^{-1}	0.688	5.7997×10^{-1}	0.164
320	4.8149×10^{-2}	1.092	1.0125×10^{-1}	0.649	5.1686×10^{-1}	0.166

Table 15: Accuracy analysis (13) for SDWLS-Linear Scheme

Grid Size	L_1 Error	L_1 Order	L_2 Error	L_2 Order	L_∞ Error	L_∞ Order
20	2.6105×10^{-1}	–	3.2012×10^{-1}	–	6.5242×10^{-1}	–
40	2.7547×10^{-1}	-0.078	3.3309×10^{-1}	-0.057	6.2006×10^{-1}	0.073
80	2.1772×10^{-1}	0.339	2.7296×10^{-1}	0.287	6.6667×10^{-1}	-0.105
160	1.1729×10^{-1}	0.892	1.7091×10^{-1}	0.675	6.1130×10^{-1}	0.125
320	5.4272×10^{-2}	1.112	1.0651×10^{-1}	0.682	4.5813×10^{-1}	0.416

Table 16: Accuracy analysis (13) for third order WENO Scheme

Grid Size	L_1 Error	L_1 Order	L_2 Error	L_2 Order	L_∞ Error	L_∞ Order
20	2.5031×10^{-1}	–	3.0966×10^{-1}	–	6.1587×10^{-1}	–
40	1.8443×10^{-1}	0.441	2.3200×10^{-1}	0.417	4.9434×10^{-1}	0.317
80	9.0391×10^{-2}	1.029	1.4733×10^{-1}	0.655	4.9213×10^{-1}	0.006
160	3.8805×10^{-2}	1.220	8.6782×10^{-2}	0.764	4.0956×10^{-1}	0.265
320	1.6053×10^{-2}	1.273	5.8798×10^{-2}	0.562	4.1746×10^{-1}	-0.028

Table 17: Accuracy analysis (13) for fifth order WENO Scheme

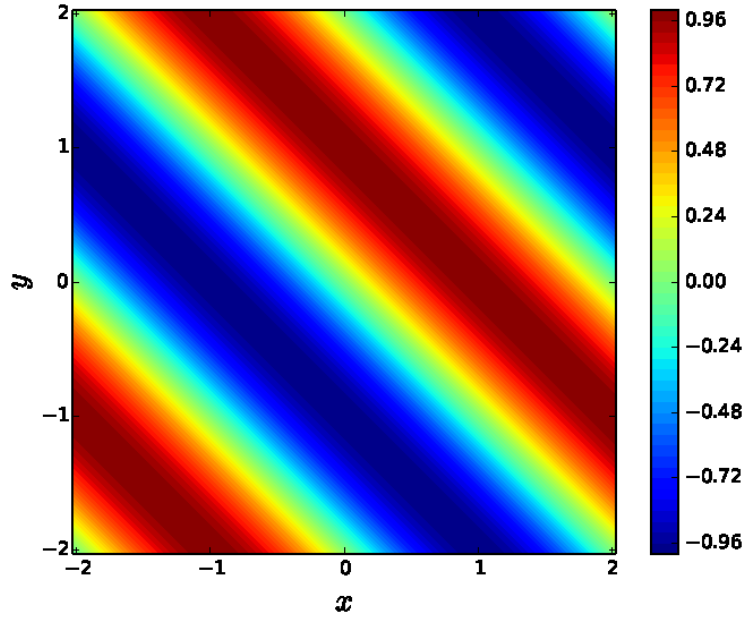


Figure 7: Exact solution of the scalar advection problem

Grid Size	L_1 Error	L_1 Order	L_2 Error	L_2 Order	L_∞ Error	L_∞ Order
40	5.4571×10^{-2}	–	6.2173×10^{-2}	–	1.1105×10^{-1}	–
80	1.4744×10^{-2}	1.888	1.8937×10^{-2}	1.715	4.2831×10^{-2}	1.374
160	3.6733×10^{-3}	2.005	5.5964×10^{-3}	1.759	1.6094×10^{-2}	1.412
320	8.9758×10^{-4}	2.033	1.6302×10^{-3}	1.779	5.9662×10^{-3}	1.432

Table 18: Accuracy analysis (2D function 15) for SDWLS-L Scheme

The exact solution of this equation is simple translation of the initial distribution with a velocity of (1,1). A standard test case [20,21] with an initial smooth distribution given by (15) is solved by using various reconstruction methods and an order of accuracy analysis is performed on structured and unstructured mesh.

$$u = \sin\left(\frac{\pi}{2}(x+y)\right) \quad -2 \leq x \leq 2; \quad -2 \leq y \leq 2 \quad (15)$$

3.2.1 Smooth sinusoidal distribution (on structured mesh)

The order of accuracy for two-dimensional formulation of the reconstruction methods is evaluated by using unsplit approach. The scalar variable is reconstructed in both directions, using the same surrounding data at time level n . The flux is calculated using the Local Lax-Friedrich Riemann solver. The evolution is done by using an explicit stability preserving three step Runge-Kutta method [24]. Since periodic boundary conditions are applied, the initial and the exact final solution are the same as shown in Figure 7. The order of accuracy calculations are displayed in Table 18 through Table 21.

Grid Size	L_1 Error	L_1 Order	L_2 Error	L_2 Order	L_∞ Error	L_∞ Order
40	5.4571×10^{-2}	–	6.2173×10^{-2}	–	1.1105×10^{-1}	–
80	2.1504×10^{-3}	4.665	2.3934×10^{-3}	4.699	3.3851×10^{-3}	5.036
160	5.2013×10^{-4}	2.048	5.7800×10^{-4}	2.050	8.1731×10^{-4}	2.050
320	1.2890×10^{-4}	2.013	1.4318×10^{-4}	2.013	2.0248×10^{-4}	2.013

Table 19: Accuracy analysis (2D function 15) for SDWLS-Q Scheme

Grid Size	L_1 Error	L_1 Order	L_2 Error	L_2 Order	L_∞ Error	L_∞ Order
40	6.7666×10^{-2}	–	7.6834×10^{-2}	–	1.3491×10^{-1}	–
80	1.7573×10^{-2}	1.945	2.4158×10^{-2}	1.669	5.3948×10^{-2}	1.322
160	4.2528×10^{-3}	2.047	7.2586×10^{-3}	1.735	2.0760×10^{-2}	1.378
320	9.8992×10^{-4}	2.103	2.1344×10^{-3}	1.766	7.8229×10^{-3}	1.408

Table 20: Accuracy analysis (2D function 15) for WENO3 Scheme

3.2.2 Smooth sinusoidal distribution (on unstructured mesh)

The equation governing the evolution of the initial conditions (15) is given by (14). The equation is solved on a unstructured mesh using the Local Lax-Friedrich (LLF) Riemann solver, using 2 Gauss-Quadrature points and a $CFL = 0.3$. The results of the accuracy analysis are displayed in Table 22. It can be observed that the L_1 error in case of SDWLS-L drops at an order of about 1.7 and in case of SDWLS-Q the error drops at an order of about 2. The SDWLS-L method does not behave very well in terms of L_∞ error as the error drops only at the rate of about 1, while SDWLS-Q maintains the order of about 2. As expected the magnitude of error in case of SDWLS-Q is smaller compared to SDWLS-L by an order of magnitude. The results from the literature [20, 21] for third order WENO and fourth order WENO show 3.0 and 4.0 respectively as the order for fine mesh. The magnitude of error of the WENO3 on fine mesh is better compared to SDWLS-Q, however on coarser mesh SDWLS-Q behaves much better, comparing the results from the literature [17] with similar mesh sizes.

3.3 Two-Dimensional Euler Equations

The general form of two dimensional conservation equations of gas dynamics can be written as,

$$\frac{\partial \mathbf{U}}{\partial t} + \frac{\partial \mathbf{F}}{\partial x} + \frac{\partial \mathbf{G}}{\partial y} = 0 \quad (16)$$

where, \mathbf{U} is the vector of conservative variables and \mathbf{F} and \mathbf{G} are flux vectors. In case of Euler equations,

Grid Size	L_1 Error	L_1 Order	L_2 Error	L_2 Order	L_∞ Error	L_∞ Order
40	9.2927×10^{-5}	–	1.0637×10^{-4}	–	1.7326×10^{-4}	–
80	3.2479×10^{-6}	4.839	3.6583×10^{-6}	4.862	6.0877×10^{-6}	4.831
160	1.4425×10^{-7}	4.493	1.6071×10^{-7}	4.509	2.5540×10^{-7}	4.575
320	9.8598×10^{-9}	3.871	1.0954×10^{-8}	3.875	1.6289×10^{-8}	3.971

Table 21: Accuracy analysis (2D function 15) for WENO5 Scheme

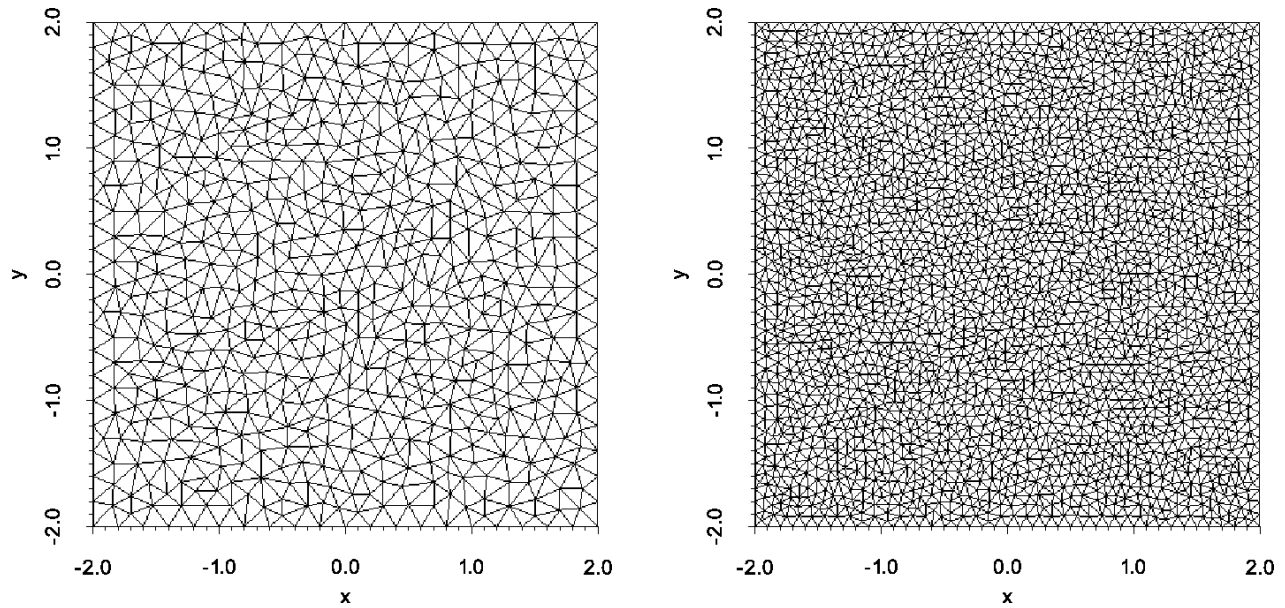


Figure 8: Mesh with 1218 and 4898 cells – for scalar advection equation

Method	Mesh Cells	L_1 Error	L_1 Order	L_∞ Error	L_∞ Order
SDWLS-L	308	1.4587×10^{-1}	–	3.4983×10^{-1}	–
	1218	6.2217×10^{-2}	1.240	1.4327×10^{-1}	1.299
	4898	1.7940×10^{-2}	1.787	5.7394×10^{-2}	1.315
	20076	4.5129×10^{-3}	1.957	2.1144×10^{-2}	1.416
	80186	1.2476×10^{-3}	1.857	1.2088×10^{-2}	0.808
	322940	4.0421×10^{-4}	1.618	6.0216×10^{-3}	1.000
SDWLS-Q	308	6.3938×10^{-2}	–	1.2679×10^{-1}	–
	1218	1.5111×10^{-2}	2.098	2.9719×10^{-2}	2.110
	4898	3.6505×10^{-3}	2.042	6.9103×10^{-3}	2.097
	20076	8.8506×10^{-4}	2.009	1.5355×10^{-3}	2.133
	80186	2.2109×10^{-4}	2.003	3.7314×10^{-4}	2.043
	322940	5.4800×10^{-5}	2.003	8.9400×10^{-5}	2.051

Table 22: 2D Linear advection problem – unstructured mesh, T=2, RK3

$$\mathbf{U} = \begin{bmatrix} \rho \\ \rho u \\ \rho v \\ \rho E \end{bmatrix}; \quad \mathbf{F} = \begin{bmatrix} \rho u \\ \rho u^2 + p \\ \rho uv \\ (\rho E + p)u \end{bmatrix}; \quad \mathbf{G} = \begin{bmatrix} \rho uv \\ \rho uv \\ \rho v^2 + p \\ (\rho E + p)v \end{bmatrix} \quad (17)$$

where, $E = \left(e + \frac{u^2 + v^2}{2}\right)$, $e = c_v T = \frac{RT}{(\gamma-1)}$, and R and γ are gas constants.

3.3.1 Isentropic vortex (on structured mesh)

The convecting isentropic vortex is a classical test problem in gas dynamics for solving Euler equations where the initial vortex travels diagonally (45° to grid lines) through the domain. This problem provides a test case for evaluating the capability of a method to retain vortex structures after long evolution in time. After one full travel cycle, the exact solution is the initial condition itself as shown in [Figure 9](#). Hence, it is an ideal problem for checking the order of accuracy of a method for system of conservation equations. The test problem is defined by a uniform flow field over which a perturbation (defining the vortex) is imposed at initial time. The uniform flow field is given as $(u_\infty, v_\infty) = (1, 1)$, $p_\infty = 1$ and $T_\infty = 1$ with the entropy defined as $S = p/\rho^\gamma$. The gas constants are given as $R = 1$, $\gamma = 1.4$ and the ideal gas law $p = \rho R T$ is used for relating the pressure, density and temperature. The perturbations imposed over this uniform flow field are given by,

$$(\delta u, \delta v) = (-y, x) \frac{\epsilon}{2\pi} \exp\left(0.5(1 - r^2)\right) \quad (18)$$

$$\delta T = -\frac{(\gamma - 1)\epsilon^2}{8\gamma\pi^2} \exp(1 - r^2); \quad \delta S = 0 \quad (19)$$

where, $\epsilon = 5$ is the strength of the vortex and $r = \sqrt{(x - x_c)^2 + (y - y_c)^2}$ is the distance from the center (x_c, y_c) of the domain. The domain of the problem is given as $[0, 10] \times [0, 10]$ with periodic boundary conditions and $(x_c, y_c) = (5, 5)$. The initial conditions to be imposed are given by $(u_0, v_0) = (u_\infty + \delta u, v_\infty + \delta v)$ and $T_0 = T_\infty + \delta T$. The isentropic condition along with the ideal gas law provides an equation for initial density given by,

$$\rho_0 = T_0^{1/(\gamma-1)} \quad (20)$$

[Table 23](#) shows the order of accuracy analysis performed using Cartesian structured grid using various methods with gradually refined grid size starting from a grid of 40×40 up to a grid of 640×640 . The values presented are the errors in ρ (density).

3.3.2 Isentropic vortex (on unstructured mesh)

The order of accuracy analysis on an unstructured mesh is performed using linear and quadratic SDWLS for the isentropic vortex problem defined above. The size of finite volume cells is maintained similar to [\[20\]](#) and [\[21\]](#) so that the results can be compared with WENO methods. The flux is integrated over the cell interfaces using 2 quadrature points. [Table 24](#) shows the results obtained for order of accuracy for SDWLS-L and SDWLS-Q. It is seen that the order of accuracy of SDWLS methods reduces slightly on unstructured mesh compared to structured mesh. This can be attributed to the first order boundary conditions applied at the boundaries, due to shortage of neighboring cells.

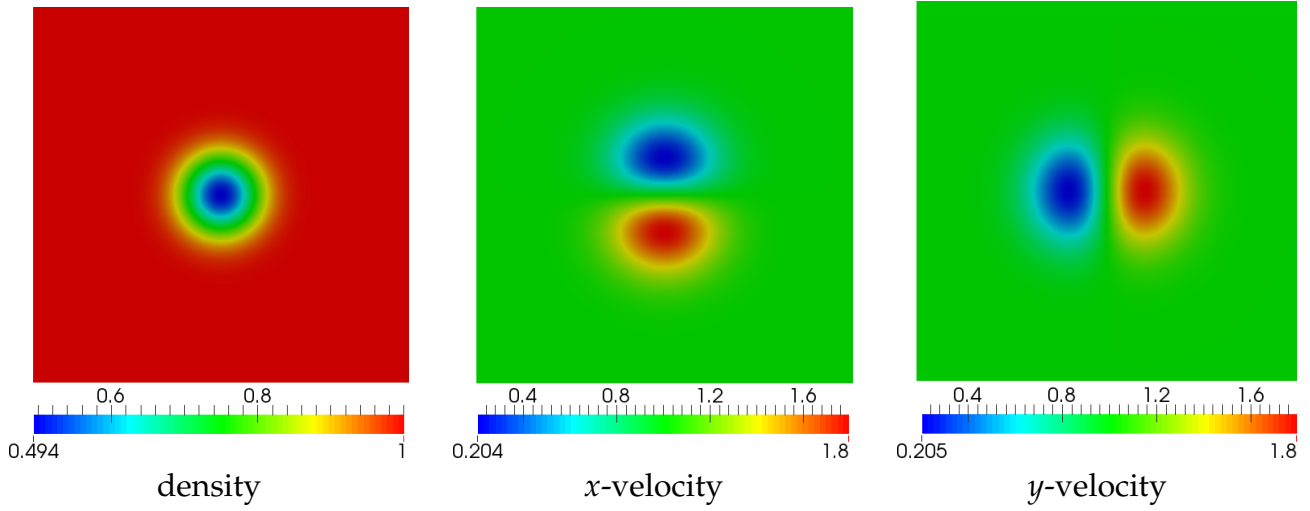


Figure 9: Solution of isentropic vortex problem

Method	Grid Size	L_1 Error	L_1 Order	L_∞ Error	L_∞ Order
WENO3	40x40	1.8648×10^{-2}	–	3.5827×10^{-1}	–
	80x80	6.7533×10^{-3}	1.465	1.3699×10^{-1}	1.387
	160x160	2.3043×10^{-3}	1.551	6.2397×10^{-2}	1.135
	320x320	9.7804×10^{-4}	1.236	3.4682×10^{-2}	0.847
	640x640	4.0724×10^{-4}	1.264	1.5401×10^{-2}	1.171
WENO5	40x40	4.5303×10^{-3}	–	8.6201×10^{-2}	–
	80x80	7.5852×10^{-4}	2.578	2.0797×10^{-2}	2.051
	160x160	1.3032×10^{-5}	5.863	2.1400×10^{-4}	6.603
	320x320	2.3729×10^{-6}	2.457	2.6636×10^{-5}	3.006
	640x640	5.8223×10^{-7}	2.027	4.3874×10^{-6}	2.602
SDWLS-L	40x40	1.6162×10^{-2}	–	3.2021×10^{-1}	–
	80x80	4.7500×10^{-3}	1.766	9.7100×10^{-2}	1.721
	160x160	1.3529×10^{-3}	1.812	5.3834×10^{-2}	0.851
	320x320	3.8434×10^{-4}	1.816	2.7490×10^{-2}	0.97
	640x640	9.2878×10^{-5}	2.049	9.4313×10^{-3}	1.543
SDWLS-Q	40x40	7.2217×10^{-3}	–	1.5153×10^{-1}	–
	80x80	1.4289×10^{-3}	2.337	2.9510×10^{-2}	2.36
	160x160	2.5447×10^{-4}	2.489	5.6347×10^{-3}	2.389
	320x320	4.3264×10^{-5}	2.556	1.0280×10^{-3}	2.454
	640x640	8.9168×10^{-6}	2.279	2.0525×10^{-4}	2.324

Table 23: Isentropic vortex problem – structured mesh, CFL=0.3, T=10, RK3

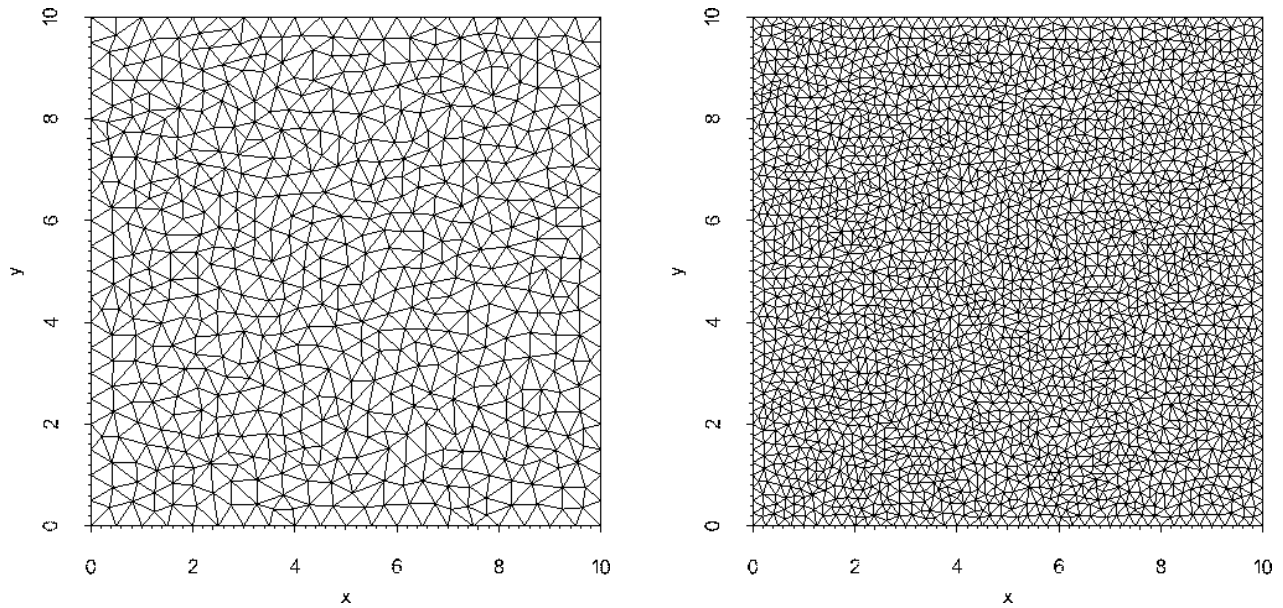


Figure 10: Mesh with 1212 and 4960 cells – Euler equations

Method	Mesh Cells	L_1 Error	L_1 Order	L_∞ Error	L_∞ Order
SDWLS-L	300	2.7387×10^{-2}	–	4.4705×10^{-1}	–
	1212	2.3037×10^{-2}	0.248	4.1500×10^{-1}	0.107
	4960	1.3521×10^{-2}	0.756	2.5222×10^{-1}	0.707
	20076	5.1255×10^{-3}	1.388	1.2212×10^{-1}	1.038
	80578	1.9941×10^{-3}	1.359	4.7943×10^{-2}	1.346
	323802	8.7036×10^{-4}	1.192	2.3380×10^{-2}	1.033
SDWLS-Q	300	2.3812×10^{-2}	–	3.9192×10^{-1}	–
	1212	8.4004×10^{-3}	1.492	1.7874×10^{-1}	1.125
	4960	1.8300×10^{-3}	2.163	4.0530×10^{-2}	2.106
	20076	3.8147×10^{-4}	2.243	8.4089×10^{-3}	2.25
	80578	7.9387×10^{-5}	2.259	1.8051×10^{-3}	2.214
	323802	1.8002×10^{-5}	2.134	3.8676×10^{-4}	2.215

Table 24: Isentropic vortex problem – unstructured mesh, CFL=0.3, T=10, RK3

References

- [1] E. F. Toro, *Riemann Solvers and Numerical Methods for Fluid Dynamics*. Berlin, Heidelberg: Springer Berlin Heidelberg, 2009.
- [2] S.K.Godunov, "A Difference Method for Numerical Calculation of Discontinuous Solutions of the Equations of Hydrodynamics," *Matematicheskii Sbornik*, vol. 47(89), no. 3, pp. 271–306, 1959.
- [3] E. F. Toro, "Viscous Flux Limiters," in *Proceedings of the Ninth GAMM-Conference on Numerical Methods in Fluid Mechanics*, pp. 592–600, 1991.
- [4] B. van Leer, "Towards the ultimate conservative difference scheme I. The quest of monotonicity," in *Proceedings of the Third International Conference on Numerical Methods in Fluid Mechanics* (R. Cabannes, Henri and Temam, ed.), pp. 163–168, Springer Berlin Heidelberg, 1973.
- [5] J. P. Boris and D. L. Book, "Flux-corrected transport. I. SHASTA, a fluid transport algorithm that works," *Journal of Computational Physics*, vol. 11, pp. 38–69, jan 1973.
- [6] D. Book, J. Boris, and K. Hain, "Flux-corrected transport II: Generalizations of the method," *Journal of Computational Physics*, vol. 18, pp. 248–283, jul 1975.
- [7] J. Boris and D. Book, "Flux-corrected transport. III. Minimal-error FCT algorithms," *Journal of Computational Physics*, vol. 20, pp. 397–431, apr 1976.
- [8] A. Harten, "On a Class of High Resolution Total-Variation-Stable Finite-Difference Schemes," *SIAM Journal on Numerical Analysis*, vol. 21, no. 1, pp. 1–23, 1984.
- [9] P. K. Sweby, "High Resolution Schemes Using Flux Limiters for Hyperbolic Conservation Laws," *SIAM Journal on Numerical Analysis*, vol. 21, no. 5, pp. 995–1011, 1984.
- [10] P. Sweby, "'TVD" Schemes for Inhomogeneous Conservation Laws," in *Nonlinear Hyperbolic Equations - Theory, Computation Methods, and Applications* (J. Ballmann and R. Jeltsch, eds.), vol. 24 of *Notes on Numerical Fluid Mechanics*, pp. 599–607, Vieweg Teubner Verlag, 1989.
- [11] P. Roe, "Some contributions to the modelling of discontinuous flows," in *Large-Scale Computations in Fluid Mechanics* (B. Engquist, S. Osher, and R. Somerville, eds.), pp. 163–193, 1985.
- [12] G. van Albada, B. van Leer, and W. Roberts Jr., "A comparative study of computational methods in cosmic gas dynamics," *Astronomy and Astrophysics*, vol. 108, pp. 76–84, apr 1982.
- [13] P. Roe, "Characteristic-Based Schemes for the Euler Equations," *Annual Review of Fluid Mechanics*, vol. 18, pp. 337–365, 1986.
- [14] B. Van Leer, "Towards the ultimate conservative difference scheme III. Upstream-centered finite-difference schemes for ideal compressible flow," *Journal of Computational Physics*, vol. 23, pp. 263–275, mar 1977.

- [15] J. Mandal and J. Subramanian, "On the link between weighted least-squares and limiters used in higher-order reconstructions for finite volume computations of hyperbolic equations," *Applied Numerical Mathematics*, vol. 58, pp. 705–725, May 2008.
- [16] J. C. Mandal and S. P. Rao, "High resolution finite volume computations on unstructured grids using solution dependent weighted least squares gradients," *Computers and Fluids*, vol. 44, pp. 23–31, May 2011.
- [17] C.-w. Shu, "Essentially non-oscillatory and weighted essentially non-oscillatory schemes for hyperbolic conservation laws," tech. rep., NASA Langley Research Center, 1997.
- [18] Z. J. Wang, K. Fidkowski, R. Abgrall, F. Bassi, D. Caraeni, A. Cary, H. Deconinck, R. Hartmann, K. Hillewaert, H. T. Huynh, N. Kroll, G. May, P. O. Persson, B. van Leer, and M. Visbal, "High-order CFD methods: Current status and perspective," *International Journal for Numerical Methods in Fluids*, vol. 72, pp. 811–845, July 2013.
- [19] D. S. Balsara and C.-W. Shu, "Monotonicity Preserving Weighted Essentially Non-oscillatory Schemes with Increasingly High Order of Accuracy," *Journal of Computational Physics*, vol. 160, no. 2, pp. 405–452, 2000.
- [20] C. Hu and C.-W. Shu, "Weighted Essentially Non-Oscillatory Schemes on Triangular Meshes," *Journal of Computational Physics*, vol. 150, pp. 97–127, 1999.
- [21] Y. Liu and Y. T. Zhang, "A Robust Reconstruction for Unstructured WENO Schemes," *Journal of Scientific Computing*, vol. 54, no. 2-3, pp. 603–621, 2013.
- [22] M. Dumbser and C.-D. Munz, "ADER discontinuous Galerkin schemes for aeroacoustics," *Comptes Rendus Mécanique*, vol. 333, pp. 683–687, sep 2005.
- [23] G. Montecinos, C. Castro, M. Dumbser, and E. Toro, "Comparison of solvers for the generalized Riemann problem for hyperbolic systems with source terms," *Journal of Computational Physics*, vol. 231, pp. 6472–6494, aug 2012.
- [24] S. Gottlieb, D. I. Ketcheson, and C.-W. Shu, "High Order Strong Stability Preserving Time Discretizations," *Journal of Scientific Computing*, vol. 38, pp. 251–289, mar 2009.